Purdue Physics REU conference
Agenda and Abstracts
August 1, 2019, room PHYS 242

9:15 **Matt Pantalon, Johann Gan.** Simulations of sawtooth-wave adiabatic passage cooling (Prof. Robicheaux)

9:40 **Timothy Nsubuga**. Analysis of Acoustic Waves during Simulation of Hydraulic Fracturing (Prof. Pyrak-Nolte)

10:00 **Justin Hazel.** *In silico* Calculation of Redox Potentials in Cytochrome bc_1 (Prof. Slipchenko. Prof. Savikhin)

10:20 – 10:30 *break*

10:30 **Yue He.** Strong Coupling Between Thermal Cesium Atoms and Nanophotonic Microring Resonator (Prof. Hung)

10:50 **Julia Kazmer.** Single Electron Backgrounds in XENON1T (Prof. Lang)

11:10 **Alexandra Kirkvold.** Artificial Photosynthesis (Prof. Pushkar)

11:30 **Nathan Chalus**. Measurement of the lifetimes of the $7p^2P_{1/2}$ and $7p^2P_{3/2}$ states of atomic Cesium (Prof. Elliott)

11:50 - 1:20 *Lunch (on your own)*

1:20 **Adina Ripin**. Finite Size Scaling for Quantum Phase Transitions in Two Electron Atoms (Prof. Kais)

1:40 **Noah Paladino.** The CMS Forward Pixel Detector Upgrade Cooling System Development (Prof. Jung)

2:00 **Helena Frisbie-Firsching.** Growth Curves of Caulobacter crescentus in a PYE to M2X Environment (Prof. Iyer-Biswas)

2:20 *The end*

6:00 - *Farewell party/picnic at Sergei Savikhin's house for REU students, advisors, speakers & significant others*
Address: 2505 McShay Dr., West Lafayette
Phone: 765-413-5026 (cell)

Simulations of sawtooth-wave adiabatic passage cooling

Johann Gan[1], Matthew Pantalon[2], Francis Robicheaux[3]

Rice University, TX[1]

Kenyon College, OH[2]

Purdue University, IN[3]

Laser cooling is a useful method for minimizing the thermal motion of particles to obtain more precise measurements. In 2018, a new method of laser cooling called sawtooth-wave adiabatic passage (SWAP) was introduced and demonstrated experimentally with Strontium-88.[1] SWAP has since been shown to be faster than traditional laser cooling techniques, and it is speculated to be more effective in cooling down certain particles that are poor candidates for other methods of laser cooling.[2,3]

SWAP works by driving a particle between a high and a low energy state, done by sweeping the laser frequency in a sawtooth pattern about the transition frequency. The absorption of a blue-shifted photon slows the particle and drives it to its high energy state. Next, a stimulated emission due to a red-shifted photon causes a second drop in momentum as well as bringing the particle back down to its low energy state.

SWAP can cool faster than traditional laser cooling methods due to its decreased reliance on spontaneous decay. An additional benefit of this decreased reliance is to mitigate the effects of having branching, meaning that the particle spontaneously decays to other "leak" states outside of the driven transition. One application of this would be for cooling antihydrogen, which is of major interest to the ALPHA collaboration in its efforts to make precision spectroscopic measurements; antihydrogen's 12% branching ratio for its 2s-3p transition makes it difficult to cool with other laser cooling methods. The laser cooling of molecules poses similar challenges due to branching. In this project, we sought to examine the effectiveness of SWAP cooling for antihydrogen and a variety of other cases.

We studied SWAP cooling in different scenarios using density matrix simulations in 1-D. For our model, we started with the Hamiltonian, Lindblad superoperator, and momentum basis states from Bartolotta et al., and added an extra internal state to represent leak states. We also added a step after each sawtooth cycle which removed coherences and allowed spontaneous decay to occur, representing a period of time between sawtooth cycles in which the laser is shut

---

[1] Matthew A Norcia, et al., 2018 *New J. Phys.* 20 023021

[2] John P. Bartolotta, et al., 2018 *Physical Review* A 98, 023404

[3] N. Petersen, et al., 2019 *Physical Review* A 99, 063414

off. For antihydrogen we used an initial momentum distribution realistic for the ALPHA experiment, which is close to thermal, but with a slightly lower concentration of particles in lower momentum states. For the rest of our simulations we used thermal momentum distributions.

There exist multiple conditions that must be met in order for SWAP to function properly. These conditions lead to an optimal configuration of the sawtooth amplitude, sawtooth frequency, and laser intensity. Due to these constraints, we optimized over these parameters for each scenario, so as to reduce the number of variables and to compare only best possible cases.

We concluded cooling antihydrogen with SWAP is infeasible. Due to various experimental constraints, the most viable transitions in antihydrogen for laser cooling are the 2s-3p transition and the 2s-4p transition. With these transitions, sustained cooling was not possible, even in the best case. The branching ratio of 12% is too low for any significant cooling to be achieved before the entire population is lost. The low recoil energy of antihydrogen may also contribute to the low quality cooling.

We then examined a range of recoil energy values, which is the only intrinsic property of a particle that matters in SWAP cooling. Our results showed that without branching, particles with higher recoil energies were cooled more quickly by SWAP. However, while such particles achieved a lower minimum velocity after sustained cooling, it was particles with lower recoil energies that achieved the lowest minimum temperature.

When we allowed leaking, higher branching ratios (less leaking) yielded better initial cooling when normalized for loss of particles. This was almost universally true, with the exception of temperatures near the cooling limits. We also found that higher recoils led to more effective cooling. Lastly, we observed a sharp drop in cooling effectiveness as the branching ratio departed from one. This suggests that SWAP cooling does mitigate the effect of leaking, but only for branching ratios close to one.

We would like to thank Professor Francis Robicheaux for his continual guidance and hands-on support. We are also grateful to Sean Myers and Troy Seberson for helpful initial discussions. This work was supported by NSF REU grant PHY-1852501 and the ALPHA collaboration.

Analysis of Acoustic Waves during Simulation of Hydraulic Fracturing

Timothy Nsubuga,

In the Rock Physics group of Prof. Laura J. Pyrak-Nolte

Purdue University, IN

Hydraulic fracturing is the process of inducing mechanical discontinuities, fractures by pumping pressurized sand, water and chemicals deep within the Earth's interior to extract natural gas. The detection of these fractures could allow for characterization of this otherwise unobservable phenomenon. Acoustic waves are compressional waves that propagate from the energy release of a material undergoing stress. The goal of my research is to determine whether acoustic emissions from transportable chemical sources can detect the presence of fractures, and if the acoustic waves can provide insight on the fracture's length or orientation of the void geometry.

The samples were fabricated using a FormLabs printer. All samples contained a central borehole for the release of chemically reactive granules that emit an acoustic signal upon dissolution. One intact sample and 3 fractured samples were printed with external dimensions of 50 mm x 50 mm x 100 mm. The fractures were composed of equally spaced tubes with elliptical cross sections. Fracture lengths varied among the samples and ranged from 1/3, 2/3 and to the full height of the sample. 18 acoustic emission sensors were placed in the same locations on each of the samples and used to record the acoustic emissions from the reactive granules. The sensors were connected to a computer through pre-amplifiers with either 100-400KHZ or 20-1200KHZ bandwidths. The Mistras Group Acoustic Emissions software was used to process the data to obtain the locations of acoustic emission events and to record the signals. The software identifies the arrival times of the signals recorded by each sensor. The time difference among the sensors is used to locate the source of an event. For each sample, 10 tests were performed. During the experiments, all events are highly localized to the borehole where the reactive granules are released.

Observation from the event location graphs for each sample shows that the event positions became less localized to the borehole when a fracture was present in the sample. This suggests that during fracture growth the accuracy of the AE software is limited likely due to the material change represented by this fracture. Examination of the signals from the intact and fractured region of the sample found that signals that propagated through a fracture had longer periods (low frequencies) than signals from the intact region .

Analysis of the event locations shows that the acoustic waves recorded by the fracture side transducers generally exhibit later arrival times and attenuation compared to those recorded by the intact side transducers. Shifting the fractures by 45° resulted in a distinct signal that suggests a connection between fracture orientation and acoustic waves.

I would like to thank Prof. Pyrak-Nolte and the Rock Physics Group for guiding my research as well as allowing me to grow. This incredible opportunity was funded by NSF REU grant PHY-1852501.

In silico Calculation of Redox Potentials in Cytochrome bc_1

Justin Hazel[1], Yongbin Kim[2], Lyudmila Slipchenko[2]

[1]Indiana Wesleyan University, Departments of Physics and Chemistry
[2]Purdue University, Department of Chemistry

Cytochrome bc_1 complex is a crucial enzyme in the electron transport chain, a process through which various compounds undergo redox reactions to push the production of ATP. In a single reaction cycle, cytochrome bc_1 oxidizes 2 ubiquinols to 2 ubiquinones and reduces of a single ubiquinone back to ubiquinol while contributing to the electrochemical proton gradient across the mitochondrial membrane. In the process of doing so, electrons are transported from substrate to substrate through the various hemes and iron-sulfur clusters present in the protein. Therefore, accurate measurement of the absolute redox potentials of these groups is greatly beneficial in understanding of the mechanism of cytochrome bc_1. Knowing the redox potentials in cytochrome bc_1 is also beneficial in answering lingering questions about differences in redox in similar proteins, such as cytochrome b_6f found in photosynthetic plants and bacterium.

This project focuses on the accurate measurement of redox potentials in cytochrome bc_1 using *in silico* methods. The protein was simulated with molecular dynamics using Gromacs software package and a modified Charmm27 forcefield. Parameters taken from literature [1] were used to simulate individual protein chains containing one or two prosthetic groups to verify system stability before simulating the full protein structure solvated in water with counter-ions. Gamess software was then used to do gas phase optimization calculations on hemes for use in hybrid QM/MM calculations. QM/MM energy calculations were then employed to calculate the energy in the protein system in various redox states, which can be used to find redox potentials using previously published methodology [2].

Classical simulations of cytochrome bc_1 solvated in water show stable energies and reasonable conformations, which suggest reasonable parameters for the numerous prosthetic groups. Future simulation with cytochrome bc_1 in a lipid bilayer are expected to show even higher stability. Gamess quantum mechanical calculations have difficulty in finding energy convergence, but current attempts show promise and may provide suitable structures for QM/MM energy calculations and analysis for redox potentials in the near future.

I would like to think Dr. Lyudmila Slipchenko, Dr. Sergei Savikhin, Dr. Danil Kaliakin, and Yongbin Kim for their insight and guidance in this project. This project was funded by NSF REU grant PHY-1852501.

References:

[1] Kaszuba, K., Postila, P.A., Cramariuc, O. et al. Parameterization of the prosthetic redox centers of the bacterial cytochrome bc_1 complex for atomistic molecular dynamics simulations. *Theor Chem Acc.* **2013,** 132, 1432-2234

[2] Tazhigulov, R.N., Gurunathan, P.K., Kim, Y. et al. Polarizable embedding for simulating redox potentials of biomolecules. *Phys. Chem. Chem. Phys.* **2019,** 21, 11642-11650

Strong Coupling Between Thermal Cesium Atoms and Nanophotonic Microring Resonator

Joey He – University of Chicago, Tzu-Han Chang – Purdue University, Chen-Lung Hung – Purdue University

Interaction between light and matter has long been a subject of interest in physics. Recent advances in nanophotonics have provided ways to probe these interactions in a growing number of regimes. The ability to produce high quality factor microring resonator cavities allows for the possibility of observing strong coupling between a cavity and thermal atoms without the need for complex trapping and cooling schemes. Such coupling will be important for the development of scalable elements of quantum networks such as optical switches.

For my project, I worked on building a vapor cell that could be used to observe this coupling using a nanophotonic microring resonator tuned to the D1 transition of cesium. I worked with my graduate student advisor, Tzu-Han, to first characterize the coupling efficiency and transmission spectra of various microring resonators. I also helped to design and build a vacuum chamber that will allow us to observe the effects of cesium vapor on the transmission spectra of the resonators isolated from any other factors.

The resonator systems are made of silicon nitride (Si_3N_4) waveguides placed on top of a silicon oxide (SiO_2) substrate. Each system consists of an array of resonators of different size near a bus waveguide. The size of each ring determines the frequency of its resonant modes. Light waves inside of the ring will destructively interfere if an integer number of wavelengths does not fit within the circumference of the ring, leading to the following relation between ring size and resonant wavelength:

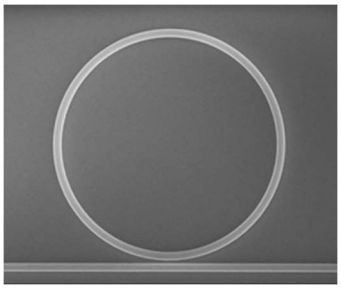

Figure 1: A single ring resonator coupled to bus waveguide

$$\lambda_m = \frac{2\,\pi\,r}{m}$$

Where *r* is the radius of the ring and *m* = 1, 2, 3…

To characterize the resonators, we measured light scattering from the resonators as well as transmission from the bus waveguide coupled to the resonators. For the both we scanned a diode laser

across the frequencies where resonances were expected. The resulting spectra were plotted and fit against a transfer matrix model in order to extract information about important parameters of the resonators such as *Q*-factor and coupling efficiency.

For apparatus design and assembly, the chamber consists of feedthroughs for electrical connections, optical fiber connections, and pumping connections. A nanophotonic chip holding the resonators and waveguides is fixed to a specially machined aluminum block, which is placed on top of a thermoelectric cooler (TEC). Since the resonant frequency of the resonator depends on its circumference, the resonators can be tuned by thermally expanding or contracting the rings. The TEC combined with a thermistor allow us to control the temperature of the rings and tune their resonances to match specific atomic transitions of cesium. High purity cesium vapor is introduced to the chamber using a SAES cesium getter dispenser.

Once complete, this vacuum chamber will provide a convenient and reliable way to observe the interactions between thermal atoms and microring cavities.

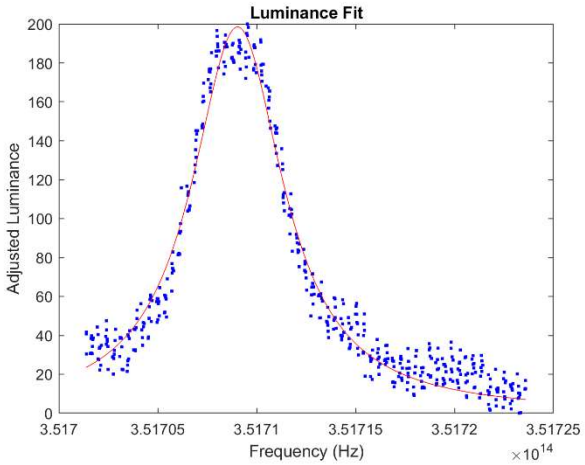

Figure 2: Fit peak of scattered light from resonator. For this particular resonator, obtained Q-factor of 2.8E6

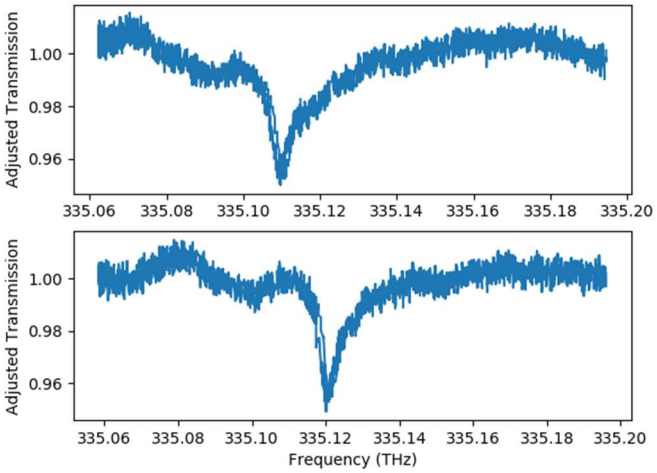

Figure 3: Thermal tuning of resonant frequency. Able to reach Cesium D1 transition frequency of 335.116 THz

Thanks to Professor Chen-Lung Hung, Cheng An, Brian Fields, Ming Zhu, and Siddhant Pandey for their help and advice with whatever problems I may encounter. Special thanks to Tzu-Han Chang who has been a huge source of support and knowledge and from whom I have learned a lot this summer. This work was supported by NSF REU grant PHY-1460899

Single Electron Backgrounds in XENON1T

Julia Kazmer, Amanda Depoian, Rafael Lang
Purdue University, IN

Most of the mass in the universe is dark matter, but dark matter particles have not yet been identified. Although there is a wide range of possible masses and properties for these particles, one leading candidate is the Weakly Interacting Massive Particle, or WIMP. XENON1T, located in Italy's Laboratori Nationali del Gran Sasso, is a dark matter detector that was searching for WIMPs until recently, when it stopped operating for the development of its successor, XENONnT. In its search, XENON1T used the photons and electrons emitted by nuclear recoils in its xenon-filled time projection chamber (TPC) shown in Figure 1. When a particle interacts with a xenon atom, photons and electrons are released. The photomultiplier tubes (PMTs) on the top and bottom of the tank immediately register the photons, which are recorded as an S1 signal. The electrons drift upward through the liquid in the TPC's electric field until they are extracted into the gas, where they scintillate and top array of PMTs record the event as an S2 signal.

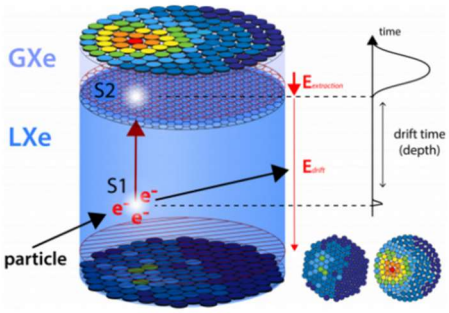

Figure 1

Since XENON1T did not detect WIMPs in the range of masses it searched, one goal of XENONnT is to improve the resolution of the detector in order to probe lower potential masses. However, major backgrounds of single electrons, called electron trains, must first be understood and mitigated in order to accurately observe and interpret the smaller signals that less massive particles would produce. These electron trains are composed of tiny S2s that can't be correlated to a specific S1, and occur across much larger time-scales than would be possible for a single interaction. It takes a maximum of approximately 1 ms for an electron released at the TPC's cathode to drift up to the gas, but Figure 2 shows that the PMTs observe single electrons entering the gas 100 ms or farther after the most recent S1. Hypotheses for the cause of this effect include long-lived excited states of xenon, electrons caught and randomly released from electronegative impurities, and a potential barrier at the liquid-gas interface preventing all the electrons from being extracted at the expected time. The hypothesis currently of most interest to our group is that of trapped electrons at the liquid-gas barrier, and we have been analyzing data taken from XENON1T in July 2018 to investigate the validity of this hypothesis.

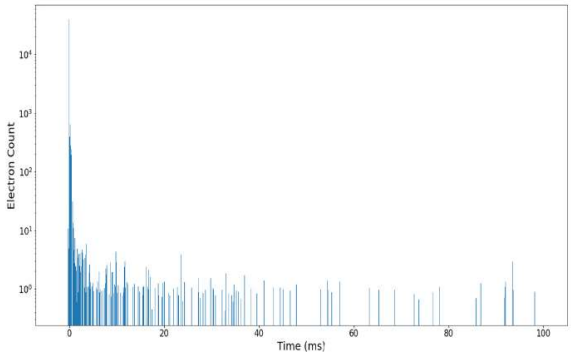

Figure 2

Our group divided the TPC into three main regions to analyze, each with different characteristics. My work focused on interactions below the cathode, where the electric field is reversed and electrons can never reach the gas. These events have S1s, but no associated S2s, and are useful to determine whether light alone can produce the effect leading to electron trains. To check for any correlation, I divided the data into groups by xy-position difference between the S1 and single electrons (Figure 3), as well as S1 size (Figure 4).

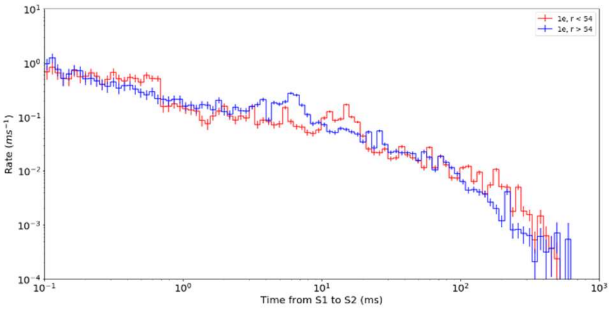

Figure 3

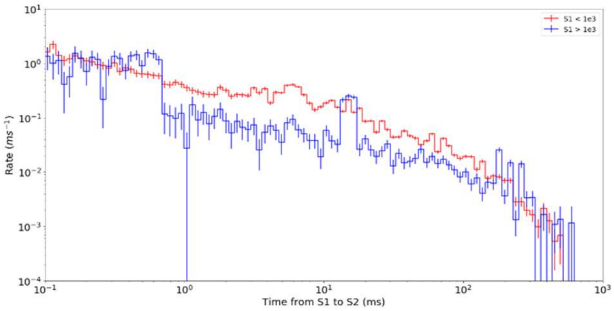

Figure 4

There does not appear to be a correlation between the rate of single electrons following S1s and either position difference or S1 size. Judging from this, it appears that the single electrons following interactions below the cathode are part of a random background that these interactions did not cause. From this information, it seems that drifting electrons are necessary to produce these backgrounds, which rules out light-induced phenomena such as photoionization. This is consistent with our expectations, as all of our current hypotheses for electron train causes at long time scales require the direct involvement of drifting electrons. This suggests it may be more useful to focus future study on predominantly events in the main liquid region of the TPC.

This work was supported by NSF REU grant PHY-1852501.

Artificial Photosynthesis

Alexandra Kirkvold[1], Scott Jensen[2], Alireza K. Ravari[2], Roman Ezhov[2], Pavani Devabathini[2], Yulia Pushkar[2]

[1]The University of South Dakota, SD, [2]Purdue University, IN

As the human population has grown, so has our demand for energy. Currently, at least 80% of the United States' energy is derived from fossil fuels, such as coal, natural gas, and petroleum.[i] These fossil fuels are an unrenewable resource; extracting them from the Earth generates pollution and harms local ecosystems. Additionally, when these fuels are burned, they emit greenhouse gases and contribute to global warming.[ii] However, for billions of years, plants and other organisms have developed photosynthesis to efficiently and sustainably harness and store energy. Photosynthesis is the conversion of solar energy, carbon dioxide, and water into fuel.

During the process of photosynthesis, Photosystem II (PSII), a photoactive metalloprotein complex found in plant cells, splits water molecules into oxygen, protons, and electrons through water oxidation. In PSII, the process begins when a photon is absorbed by the chlorophyll and one of its electrons is promoted to a higher energy. This electron is then passed down to the other parts of the reaction center: plastoquinone A and plastoquinone B. Once enough energy has accumulated, the small quinone is released from the photosystem and is delivered to the next step in the electron transfer chain. Because this leaves the original chlorophyll without an electron, it takes one from a water molecule.[iii] The oxygen-evolving center in PSII uses the Mn_4O_5Ca cluster to remove four electrons from two water molecules, creating oxygen gas (O_2) and four hydrogen ions ($4H^+$). Finding out how the dynamics and chemistry of this process work is extremely important to use artificial photosynthesis.

Many different metal complexes have been studied as an alternative for natural photosynthesis. Our group uses Ruthenium (Ru) based catalysts because they are of the most studied and efficient for the water splitting process. To do this, I measured the rate of oxygen production of each catalyst after Cerium Ammonium Nitrate (CAN) was added. Adding the CAN oxidizes the Ru complex and, in this case, brings Ru^{II} to higher oxidation states which are active catalysts. An excessive amount of CAN is required to go through the complete cycle and release oxygen molecules. Measuring the oxygen production was achieved by using a Clark type electrode called an oxygraph. This machine reduces oxygen at the cathode, which requires a steady stream of electrons to the cathode. This is directly dependent on the rate at which oxygen can reach the electrode's surface; so, if the amount of oxygen being reduced is increasing, so is the current through the electrode. The graph of the signal, after being calibrated, is therefore the graph of the oxygen being produced.

Part of my project was determining the difference between oxygen production rates of Ru complexes in H_2O and D_2O. One such complex was $(bpy)_2Ru(bpyNO)(PF_6)_2$, of which I made

specific concentrations (1mM) in H_2O and D_2O, added CAN, then measured the oxygen production in the oxygraph. A graph from one of my tests is shown below. As you can see, there is a higher rate of oxygen production in D_2O, indicating that it demonstrates the reverse Kinetic Isotope Effect and gives us information about the dynamics of the reaction.

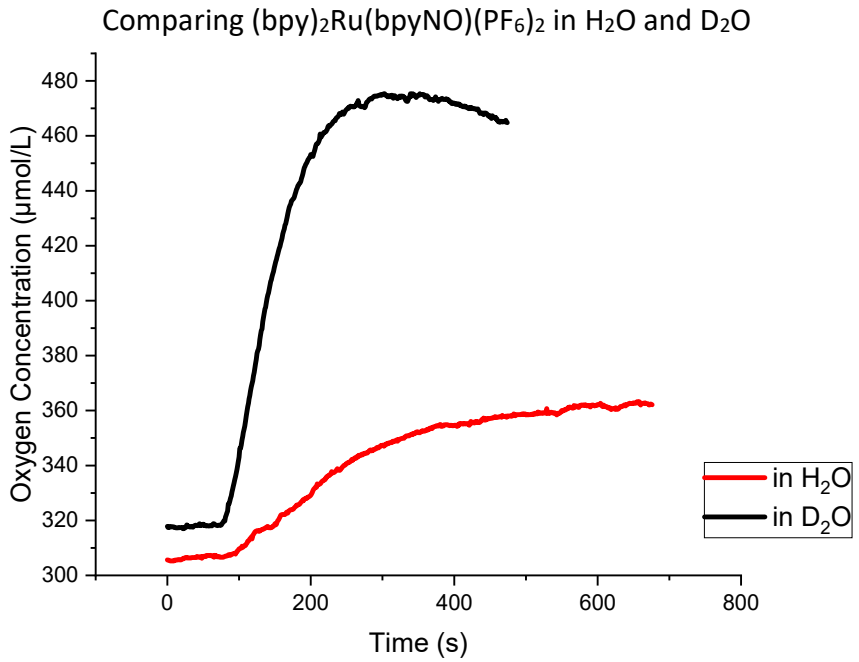

I am so incredibly grateful that I had the opportunity to complete this research at Purdue. I have learned and grown so much as the result of this REU. I would like to thank Professor Yulia Pushkar for welcoming me into her lab and providing me invaluable advice and mentorship. I would also like to thank Scott Jensen, Ali Ravari, Roman Ezhov, and Pavani Devabathini for their constant support through the summer. This work was supported by NSF REU grant PHY-1852501.

Measurement of the lifetimes of the $7p^2P_{1/2}$ and $7p^2P_{3/2}$ states of atomic Cesium

Nathan Chalus[1,2], George Toh[3,4], Andrew Burgess[2], Amy Damitz[2,3], Poolad Imany[3,4], D.E. Leaird[3,4], Carol E. Tanner[5], Andrew M. Weiner[3,4], and D.S. Elliott[2,3,4]

[1]*Department of Physics, Southern Illinois University Edwardsville, Edwardsville, Illinois 62026, USA*
[2]*Department of Physics and Astronomy, Purdue University, West Lafayette, Indiana 47907, USA*
[3]*Purdue Quantum Science and Engineering Institute, Purdue University*
[4]*School of Electrical and Computer Engineering, Purdue University*
[5]*Department of Physics, University of Notre Dame, Notre Dame, Indiana 46556, USA*

Over the past several years, good progress has been reported in determining to high precision electric dipole (E1) matrix elements for transitions between low-lying energy levels of atomic cesium. These measurements are motivated by investigations of parity non-conservation in cesium, which depend upon precise determinations of these matrix elements, as well as of matrix elements for the weak force. Agreement between E1 matrix elements calculated using powerful coupled-cluster theoretical techniques and experimental results determined through a variety of laboratory techniques is excellent at the 0.2% level. While most measurements of E1 matrix elements involve the ground state, matrix elements between two excited states are also useful tests of theory.

Our goal this summer was to measure the lifetimes of two separate excited states of cesium, specifically the $7p^2P_{1/2}$ and $7p^2P_{3/2}$ states. We excite a cesium atom from its ground $6s^2S_{1/2}$ state to either its $7p^2P_{1/2}$ or $7p^2P_{3/2}$ and collect the light emitted from the cesium atom. This allows us to experimentally measure the lifetimes for these two excited states. However, due to the different decay paths the atom can take back to its ground state (Figure 1), this can be quite a challenge. We isolate and collect the light indicated by the purple decay line in figure 1. We use a technique known as Time Correlated Single Photon Counting (TCSPC) used in chemistry and biology. We excite the atoms with a pulse of laser light and create a high-resolution histogram of number of photons versus photon arrival time. By fitting this decay curve to a double exponential, we can then extract the $7P_j$ lifetimes.

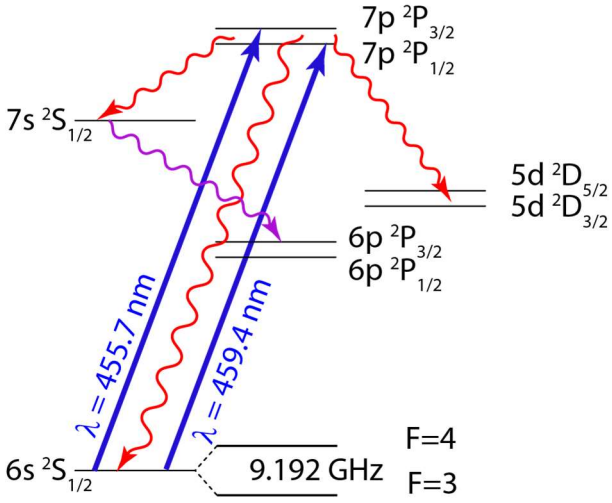

Figure 1. Plot of the energy levels of cesium relevant to the lifetime measurement.

During my summer REU experience, I have set up various components on the optical table for this lifetime experiment. Over the past ten weeks, I collected over 80 hours of data, resulting in close to

~80 data sets which were each individually analyzed and used to make the two separate lifetime measurements. An example of one of these data sets is given below in figure 2.

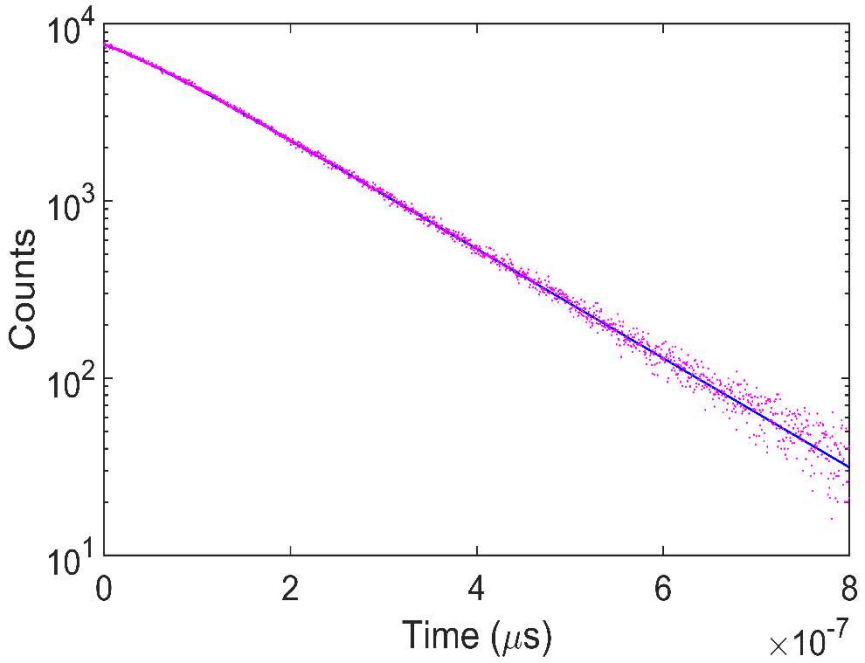

Figure 2. Sample histogram of photon counts vs photon arrival time. The purple dots are experimental data and the blue line represents the curve of best fit. This histogram consists of 15 min of recorded data and shows the exponential decay of fluorescence.

We believe to have significantly reduced the amount of uncertainty of both $7p^2P_j$ lifetimes. In addition, this summer served to be fruitful by giving me more experience analyzing data and discussing and thinking about systematic errors which may affect the accuracy of the measurements. In addition, this summer gave me a chance to work collaboratively with graduate students and postdocs from another lab. With previous authors reporting values with uncertainties close to 2-3%, we have made good progress obtaining uncertainties >0.1%, an order of magnitude improvement compared to past results. This new level of precision is useful, because it allows theorists to check weak charge calculations to a greater level of precision.

Acknowledgements: I would like to thank Prof. Daniel S. Elliott for guiding me and granting me the opportunity of working with him during this Summer Internship program. Special thanks to the program coordinators for granting me the opportunity of taking part in this wonderful experience. This work was supported by NSF REU grant PHY-1852501 and PNC grant PHY-167603.

Finite Size Scaling for Quantum Phase Transitions in Two Electron Atoms

Adina Ripin, Teng Bian, Sabre Kais

Purdue University, West Lafayette IN

While normal computers operate using classical bits to store information, quantum computers are able to use principles from quantum mechanics such as entanglement and superposition to model quantum systems. For quantum chemists, one of the most exciting applications of quantum computers would be performing electronic structure calculations for large atoms and molecules, long considered the "holy grail" of the field.

Previous papers have shown that there exists an exact mapping between the electronic structure Hamiltonian and the Ising Hamiltonian. This Ising type Hamiltonian can be easily implemented/initialized on current quantum hardware, and could theoretically be used to solve for the ground state and ground state energy of systems larger than can currently be computed on a classical computer.

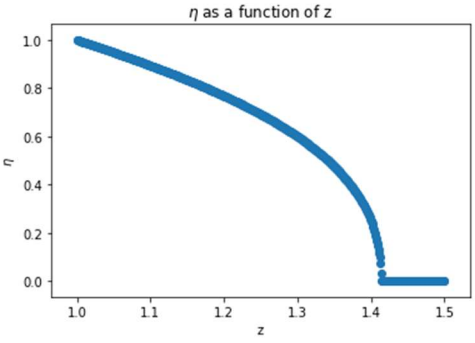

Figure 1

In the field of electronic structure calculations, symmetry breaking is analogous to quantum phase transitions, and lead to materials displaying various interesting properties. Quantum phase transitions can also tell us a lot about the stability of certain states. In the large D limit, for a two electron atom, there is a clear phase transition as the nuclear charge z is decreased, which is the point at which one of the electrons becomes unbound. This transition can be seen in Figure 1, where the parameter η is $\frac{r_1-r_2}{r_1}$. The Hamiltonian for this system is $\mathcal{H} = \sum_{i=1}^{N} \frac{n_i^2}{2r_{ni}^2} - \sum_{i=1}^{N} \frac{Z}{r_{ni}} + \sum_{i=1}^{N} \sum_{\square=1}^{N} J_{r_{ni},r_{nj}}(r_{ni}, r_{nj})$. The second quantization of this form then becomes $\mathcal{H} = \sum_{i,j=1}^{N} h_{ij} a_i^\dagger a_j + \frac{1}{2}\sum_{i,j,k,l=1}^{N} h_{ijkl} a_i^\dagger a_j^\dagger a_k a_l$, where $h_{ij} = \int dx\, \chi_i^*(x)(\frac{1}{2x^2} - \frac{Z}{x})\chi_j(x)$ and $h_{ijkl} = \int dxdy\, \chi_i^*(x)\chi_j^*(y)J_{x,y}(x,y)\chi_k(y)\chi_l(x)$ and our set of basis functions are simple delta functions. We can then write use a Jordan Wigner transformation to write the Hamiltonian in terms of spin operators, and write it as an Ising type Hamiltonian, which can be seen in Figure 2.

$$\mathcal{H} = h_{11}\frac{1-\sigma_z^{(1)}}{2} + h_{22}\frac{1-\sigma_z^{(2)}}{2} + h_{1221}\frac{1-\sigma_z^{(1)}}{2}\frac{1-\sigma_z^{(2)}}{2}$$
$$= \frac{h_{11}}{2} + \frac{h_{22}}{2} + \frac{h_{1221}}{4} - (\frac{h_{11}}{2} + \frac{h_{1221}}{4})\sigma_z^{(1)} - (\frac{h_{22}}{2} + \frac{h_{1221}}{4})\sigma_z^{(2)} + \frac{h_{1221}}{4}\sigma_z^{(1)}\sigma_z^{(2)}$$

Figure 2

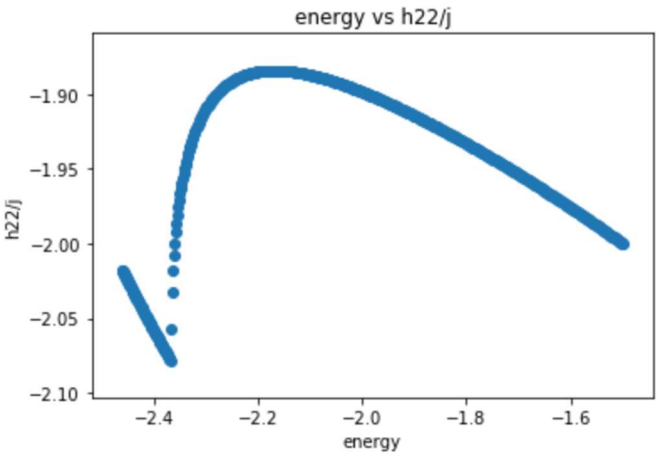

Figure 3

The parameters of this Ising Hamiltonian can be shown to have properties of the quantum phase transition as well, as shown in Figure 3, in which the parameters h_{11}/h_{1221} are plotted against the energy of the system. The fact that we can see this phase transition in qubit space is very promising.

Analytically, these critical z values have been found for atoms up to n=4 electrons in 3 dimensions. For larger systems, these calculations become incredibly unwieldly, and investigating them using quantum computation would be a useful tool to further understand them since we showed that theoretically, quantum phase transitions can be mapped into qubit space.

Acknowledgements: This work was supported by NSF grant 1852501. Thank you to Professor Kais for welcoming me into his group and his guidance and knowledge. Thank you also to Teng Bian for all his help.

The CMS Forward Pixel Detector Upgrade
Cooling System Development

Noah Paladino[1], Ryan Story[2], Andrew Wildridge[2], Abraham Kosky[2], Souvik Das[2], Andreas Jung[2]

[1]Rutgers University, NJ, [2]Purdue University, IN

Introduction

The Large Hadron Collider (LHC) is the world's premier particle accelerator, probably best known for the 2012 discovery of the Higgs boson. Located on the border of France and Switzerland at CERN, it accelerates protons through a 27 km long tunnel to a center of mass energy of 13 TeV. One of the experiments located along the ring is the Compact Muon Solenoid (CMS), a general purpose detector designed to study the Standard Model and look for new physics. It generates a 4 T magnetic field to bend the path of particles moving transverse to the beamline and aid in particle detection and identification. Purdue University in particular is responsible for designing and manufacturing a significant fraction of parts for the forward pixel detector (depicted at right), intended to "track" charged particles that escape at angles close to the beamline (small eta in eta-phi space). Data from the forward pixel detector is important for determining pileup and luminosity for the detector. Cooled by two-phase CO_2, the detector is being upgraded during the present long shutdown to have increased radiation tolerance and more disks for better coverage.

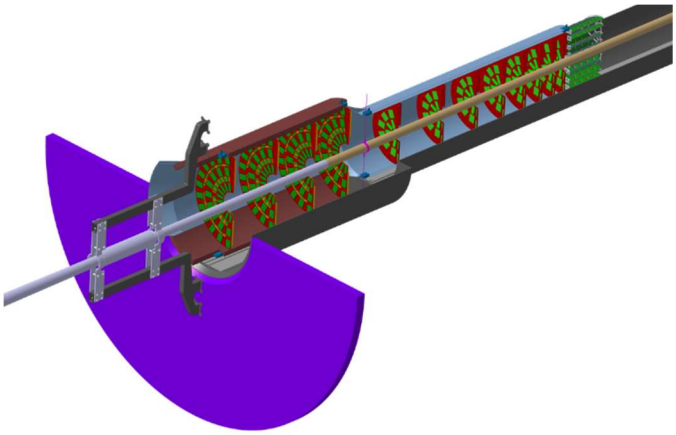

In-Plane Thermal Conductivity Testing

Each of the pixel detectors will be mounted on carbon fiber sheets, and it is essential to ensure good thermal conductivity to wick heat away from the chips. Otherwise, the waste heat from operating the pixel detector (about 40 kW) will force the detector into thermal runaway. Purdue University's Silicon Detector Laboratory has designed and optimized a customized device to measure the thermal conductivity of carbon fiber samples with fibers both parallel and perpendicular to the heat flow. A heater and water-cooling block are used to establish a thermal gradient across the sample, held in place by copper blocks. Thermistors embedded in the copper measure the thermal gradient to determine the temperatures at each end of the sample under test. In particular, I was responsible for helping to assemble the apparatus, as well as for designing and constructing the pressure application mechanism. My design included

springs mounted on a threaded rod to allow a consistent amount of pressure to be applied, no matter the sample length, even upwards of 5.5 cm.

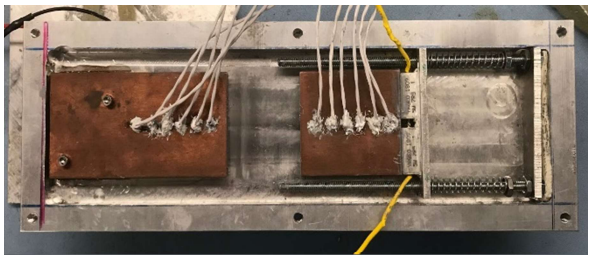

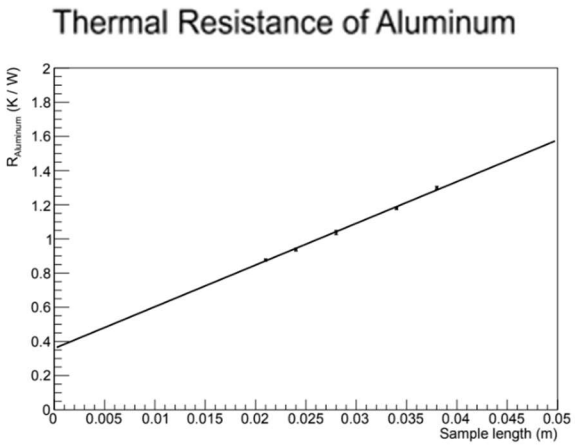

In addition to the design and construction of the apparatus, I also worked on taking measurements of the thermal conductivity of different materials. In particular, I focused on calibrating the device using samples of aluminum and copper of varying lengths. After receiving machine shop training, I was able to ensure the samples were flat to within 30 µm, ensuring good thermal contact with the apparatus. Using data from the thermistors, one can determine the heat flux through the sample, q, using Fourier's law: $q = -k\nabla T$, where k is the known thermal conductivity of the copper and ∇T is the temperature gradient. Extrapolating from this information, we can plot how thermal resistance of a sample varies with sample length and fit a line to the results, thus yielding the in-plane thermal conductivity of a given sample.

Mixed-Phase CO_2 Cooling Setup

A test cooling system with a mixed-phase CO_2 refrigerant is setup to monitor how well the carbon fiber can deposit waste heat to be carried away. The energy is absorbed in the latent heat of vaporization of the CO_2 as it travels through the carbon fiber panel with a simulated device mounted on it inside the coldbox itself. The whole setup is depicted in the image at right.

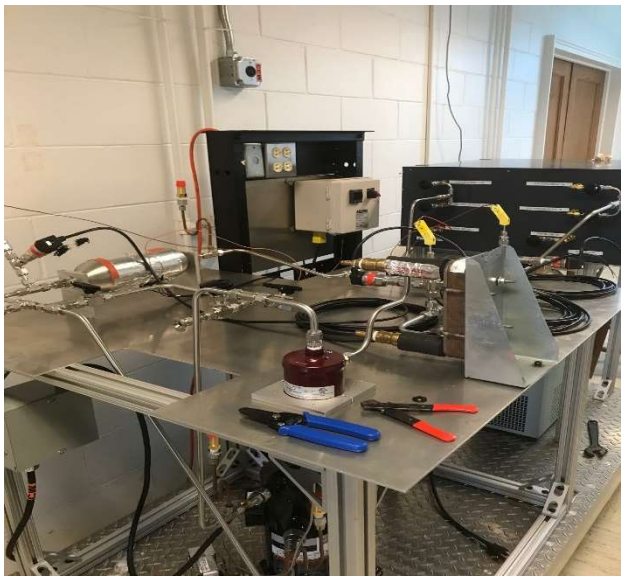

My primary responsibility was to design an intuitive monitoring system using thermocouples and pressure sensors embedded in the coolant loop, as well as thermistors on the device under test itself. To accomplish this task, I wrote a Python script to communicate with a Keithley 2701 multimeter and record the state of the system every 5 seconds. The script, known as the Coldbox Remote Monitor (CRM) also starts a web server where I designed a website to act as a user interface. An example of the monitoring webpage showing a simulated run is depicted below.

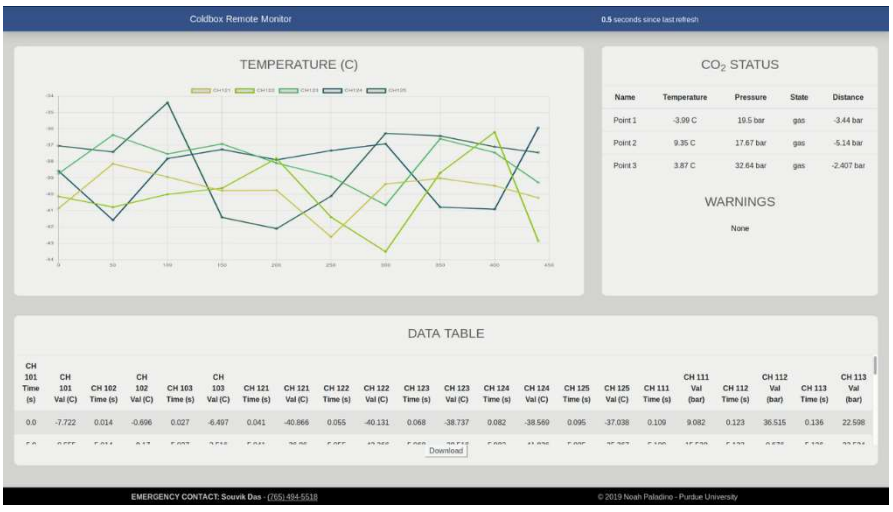

In addition to the live monitoring, the system stores data on disk to allow for easy analysis after the completion of the experiment. The focus of this data analysis would be on characterizing effects such as thermal runaway of the system. This setup would also help test new and innovative designs like micro-channel cooling.

Alongside this project, I developed a Python package, now available in the official repositories, called py2700, that allows users to interface with Keithley 2700 series digital multimeters. It offers the most common functionalities available in a program like NI LabView or Keithley Kickstart. Using this package, users can quickly and simply develop data logging scripts in Python for a variety of applications.

Acknowledgements

First and foremost, I would like to thank Professor Jung as well as everyone at Purdue's Silicon Detector Laboratory for all their assistance and support throughout the project. I also would like to thank the Purdue University Physics Department for the facilities to perform this research and the NSF REU program for providing the opportunity to do this work. In particular, I would like to acknowledge the support of NSF REU Grant PHY-1852501 that has made this program possible.

Growth Curves of *Caulobacter crescentus* in a PYE to M2X Environment

Helena Frisbie-Firsching[1], Michael Carlson[2], Srividya Iyer-Biswas[2]

[1]Haverford College, PA, [2]Purdue University, IN

C. crescentus grows with an exponential growth curve that scales based on a temperature-dependent cellular level timescale.[1] The dependence of the timescale on the available nutrients of the growth environment is a new avenue of investigation. By comparing the timescale of *C. crescentus* in an environment with peptone yeast extract (PYE) as the nutrient source to the timescale in an environment with minimal media with xylose (M2X), as well as the intermediate timescales as *C. cresentus* acclimates to the M2X environment, the potential of nutrient-dependence for cellular timescales can be established. Improved understanding of the ways in which growth curves are scaled and otherwise affected by different environmental factors may make it possible for these timescales to be manipulated to control cell populations.

In this experiment, C. crescentus is initially in an environment with PYE as the nutrient source. A little over 400 minutes into the experiment, after consistent growth curves for the PYE environment are achieved, the nutrient source is switched to M2X. The growth curves of *C. crescentus* change at that point in time, and transition to beginning to display a different, consistent growth curve. Initial results suggest that the length of time taken to establish a new growth curve is dependent on the life stage of *C. crescentus* at the time of the switch to M2X. *C. crescentus* bacteria that were at earlier life stages at the time of the switch generally took less time than *C. crescentus* at mid to late life stages to display a new, consistent growth curve. Another observation of note is that almost 38% of *C. crescentus* exceeded the average cell size established in the PYE media immediately after the switch to M2X. The reason behind this behavior is uncertain and requires further investigation, though it was observed with more frequency in *C. crescentus* at mid life stages when the switch to M2X occurred.

The initial results of this experiment suggest that further investigation into the post-switch *C. crescentus* growth curves is of interest. By repeating the experiment and letting the experiment

run for a longer period of time, a more precise evaluation of the growth curves in a post-switch M2X environment can be completed, since in this experiment the M2X growth curve was only beginning to be established.

Thank you to David Lamey, Ferdinand Ziegler, Michael Carlson, and Professor Srividya Iyer-Biswas for their invaluable instruction and assistance. An additional thank you to the National Science Foundation for funding my research experience through the REU grant PHY-1852501.

---

[1] Iyer-Biswas S, Wright C, Jonathan H, Lo K, Stanislav Burov, Yihan Lin, Gavin E. Crooks, Sean Crosson, Aaron R. Dinner, Norbert F. Scherer (2014) Scaling laws for single cells. *Proceedings of the National Academy of Sciences* 11 (45) 15912-15917

---

[i] Energy Information Administration (EIA). 2019. Monthly Energy Review - July 2019. Washington, DC: US Department of Energy. doi:EIA-0035(2019/7).

[ii] Energy Information Administration (EIA). 2015. U.S. Energy-Related Carbon Dioxide Emissions, 2014. Washington, DC: U.S. Department of Energy.

[iii] Protein Data Bank (PDB). 2004. Photosystem II. doi:10.2210/rcsb_pdb/mom_2004_11.